



Delta Journal of Science  
Available online at <https://djs.journals.ekb.eg/>



Research Article

**CHEMISTRY**

## **Fe<sub>3</sub>O<sub>4</sub>@ZnO core-shell nanoparticle development for drug delivery application**

**Abdelhamid M. El-Sawy, Hoor M. Azab , Mohamed Y. El-Sheikh and El Zeiny M. Ebid**

Chemistry Department, Faculty of Science, Tanta University, Tanta, Egypt

Corresponding author :Hoor Mohamed

e-mail: [hoormohamed437@gmail.com](mailto:hoormohamed437@gmail.com)

Received: 15/6/2022

Accepted: 5/9/2022

### KEY WORDS

### ABSTRACT

Doxorubicin  
(DOX), Zinc  
oxide/ Magnetic  
Nanoparticles,  
Core/Shell  
Nanoparticles,  
Drug Delivery  
System and  
ultrasonic,  
Photodynamic  
therapy

Developing a drug delivery system to target diseased areas attracted considerable attention. The system should achieve its desired therapeutic effect without side effects.

ZnO nanoparticles display great efforts in photodynamic therapy (PDT), due to the ability to generate reactive oxygen species (ROS), Cancer cells are expected to die without damaging healthful cells.

The developed system to deliver the drug is magnetite zinc oxide nanoparticles (Fe<sub>3</sub>O<sub>4</sub>@ZnO) core shell system. Scanning electron microscopy (SEM) showed formation of magnetite with a unified spherical nanoparticle with core size equal 25±5 nm. The average size for magnetite zinc oxide nanoparticles (Fe<sub>3</sub>O<sub>4</sub>@ZnO) after functionalization with (3-aminopropyl) triethoxysilane (APTES) and loading drug is about 120±10 nm. Transmission electron microscopy (TEM) image shows the uniform size of the core-shell. The core size of magnetite is equal 25 ± 5 nm, and for zinc oxide shell is equal 95 ± 15 nm. To mimic the blood pH, drug release has been studied in phosphate buffer solution (PBS) at pH 7.4.

Besides the mechanical stirring method, ultrasonication was used as external stimuli of drug release. Constant weight of Fe<sub>3</sub>O<sub>4</sub>@ZnO loaded with the drug was put into buffer (pH = 7.4). Then, the sol was agitated using ultrasonication. The system follow zero order kinetic in both external stimuli. In conclusion, the developed system has been synthesized as a core /shell drug delivery system using ultrasonication method. The time of drug-release upon using ultrasonication is five times faster than that caused by mechanical stirring under the same experimental conditions.

## Introduction

Cancer is a deadly illness in which cells multiply abnormally and invade nearby tissues, causing severe disease and destroying healthy cells. There are many ways to treat cancer, such as chemotherapy, radiation, and immunotherapy, and these treatments have proven effective in many types of cancer.

Unfortunately, chemotherapy does not affect the affected part only, but also affects healthy cells, as it uses drugs to kill cancer cells. It targets cells that multiply rapidly. But, some cells multiply at a high average as well in our bodies, such as skin cells, bone marrow, and endothelial cells. Therefore, chemotherapy may affect these cells as well. To reduce these side effects, we resort to a combination of chemotherapy and nanotechnology.

In biomedical applications, such as drug delivery and disease diagnosis, nanoparticles (NPs) are used (**Watermann and Brieger, 2017**). Because of the unique properties possessed by magnetic nanoparticles (MNPs), their large surface area, small size, quantum properties, and other properties, make them useful and attractive for medical applications. Magnetite nanoparticles are very popular in biomedical applications as they are a metabolic system. Modifying the surface of magnetite nanoparticles could make them more biocompatible in biomedical applications (**Zada et al., 2016**).

Photodynamic therapy (PDT) includes the presence of a local photosensitizing

factor in the tumor, which may require the synthesis of a metabolic system followed by its stimulation by light of a certain wavelength. PDT causes a series of photochemical processes that cause photodamage to tumor tissue. It can generate reactive oxygen species (ROS) in the presence of a beam of light. ZnO nanoparticles are of great importance in PDT. Zinc oxide (ZnO) nanoparticles produce some phototoxicity that efficiently kills cancer cells. Several reports have used zinc oxide magnetite nanoparticles for drug delivery. Cancer cells are expected to die without harming healthy cells. But this application shows slightly poor releasing of the drug from the system with long release periods reaching 72 h (**Keshavarz et al., 2020**).

Ultrasound is considered a promising application as an external trigger for drug release. In this research, ultrasonication has been used as external stimuli for drug release from the Fe<sub>3</sub>O<sub>4</sub>@ZnO system to make a highly effective system for cancer tumor tissue and easy to release drug with no side effects on normal tissues (**Moorthy et al., 2017**).

To deliver the drug to infected cells, this study prepared a multifunctional system composed of magnetite as a core enclosed by an outside layer of zinc oxide. One of the most common particles used to deliver the drug is iron oxide nanoparticles (**Xiao, and Xiao, 2009**). Because it is one of the

metabolic systems that can be exerted through metabolic pathways, it is easily manufactured in the nanoscale range and has superior magnetic properties. On the other hand, ZnO nanoparticles are important as effective drug delivery systems due to their optical properties (Yi, *et al.*, 2005). The structures are highly ordered in addition to being chemically and thermally stable, biocompatible and non-toxic.

In the present study, magnetite Fe<sub>3</sub>O<sub>4</sub> was synthesized by using ultrasonication method giving grains with a uniform spherical shape of mean size  $25 \pm 5$  nm. Fe<sub>3</sub>O<sub>4</sub> grains were used as a core then coated with zinc oxide shell giving Fe<sub>3</sub>O<sub>4</sub>@ZnO core shell system. The Fe-O and Zn-O are characterized by XRD and FT-IR spectroscopy. To promote interfacial behavior of our inorganic oxides system we have decorated this shell with an amino group by using (3-aminopropyl) triethoxysilane (APTES) followed by loading doxorubicin anticancer drug (DOX) on the surface of the system. The whole mean size for the particles was about  $120 \pm 10$  and this is considered a good size in nano applications. The system that was developed shows good loading efficiency, less toxicity and faster drug-releasing upon applying ultrasonication as a new releasing method. The system also enhancing the anticancer performance of doxorubicin at low doses for breast cancer treatment, this leads to less doses of drug and less harmful.

## EXPERIMENTAL

### Chemicals

Iron (II) sulfate heptahydrate (FeSO<sub>4</sub>.7H<sub>2</sub>O), sodium hydroxide (NaOH), ethyl alcohol (C<sub>2</sub>H<sub>5</sub>OH,99%), ammonia (NH<sub>4</sub>OH, 0.25 M) were obtained from piochem Chemicals Co, cetyl trimethyl ammonium bromide (CTAB), (3-aminopropyl) triethoxysilane (APTES), it has a density of 0.946 g/ml, was purchased from Sigma-Aldrich, phosphate buffer solution (PBS), doxorubicin hydrochloride C<sub>27</sub>H<sub>30</sub>ClNO<sub>11</sub> (DOX) anticancer drug from RMPL PHARMA LLP and zinc acetate were analytical grade chemicals and used without any purification.

### Characterization techniques

Magnetite/zinc oxide nanoparticles (Fe<sub>3</sub>O<sub>4</sub>@ZnO) were analyzed by using X-ray powder diffraction (GNR X-ray diffractometer /APD 2000 PRO) with Cu anode, line focus ( $\lambda = 1.540562 \text{ \AA}$ ) in the  $2\theta$  range from 10 to 90 with step size 0.050. Fourier- transform infrared spectroscopy (FTIR) was used to record the FTIR spectra of the samples using the potassium bromide (KBr) pellet technique. A small portion of the sample was mixed well with a small portion of KBr powder in a mortar, and then the mixture was analyzed by FTIR Thermo-Nicolet FTIR Avatar 370. Thermogravimetric analysis (TGA) was carried out using Shimadzu TG-50 thermal analyzer (Japan) from 30 to 700 °C under a nitrogen atmosphere, 5-10 mg of each sample was located separately in the TGA instrument (TGA-50) pan to record the

weight residue with increasing temperature at a heating rate of  $5\text{ }^{\circ}\text{C min}^{-1}$  under a nitrogen atmosphere with a gas flow of  $10\text{ ml min}^{-1}$ . The magnetization behavior was measured by a home-made vibrating sample magnetometer (VSM), Department of Physics, Faculty of Science, Tanta University in an external magnetic field ranging from  $-10\text{ kOe}$  to  $+10\text{ kOe}$  (El-Alaily *et al.*, 2015). The ultrasonic instrument is DAIHAN-brand<sup>®</sup> Analog Ultrasonic Cleaners, WUC-A, with a frequency of 28/40 kHz and heating power of 172 W. Inductively coupled plasma - optical emission spectrometry (ICP-OES) Optima 7000 DV (Perkin Elmer) with a double monochromator and simultaneous CCD array detector was used to determine the concentrations of Zn and Si (251.61 nm) concentrations.

#### Preparation of magnetite ( $\text{Fe}_3\text{O}_4$ )

For the synthesis of magnetite nanoparticles, 2.31g of  $\text{FeSO}_4 \cdot 7\text{H}_2\text{O}$  is solved in 90 ml of purified water using a magnetic stirrer for 10 min and then sonicated using an ultrasonic instrument for 75 min. After 15 min from the start of the ultrasonic treatment, 9 ml of sodium hydroxide at a concentration of 3 M is added to the reaction. After the reaction is complete, the black precipitate of  $\text{Fe}_3\text{O}_4$  is washed several times with water and last time with ethanol, then the slurry is collected using a magnet and then dried in an oven at  $80^{\circ}\text{C}$  overnight (Abbas *et al.*, 2013).

#### Preparation of $\text{Fe}_3\text{O}_4@ZnO$ core-shell

0.125mg of above-synthesized magnetite nanoparticles were dispersed in 130 ml of water by ultra-sonication for 30 min. Then zinc acetate (50 ml of 0.08M) was dropped (drop by drop) into the above mixture. Then, when the reaction temperature was raised to  $40^{\circ}\text{C}$ , 20 ml of 5 % ammonia (by weight) (2.94 moles) were poured into the beaker. The resulting mixture was further allowed for sonication for another 30 min. The resulting precipitate was collected by using centrifuge at 10,000 rpm for 5 min. Finally, the precipitate was dried at  $80^{\circ}\text{C}$  (Beltran-Huarac *et al.*, 2010; Shen *et al.*, 2012).

#### Functionalization of $\text{Fe}_3\text{O}_4@ZnO$ core-shell nanoparticle with APTES

$\text{Fe}_3\text{O}_4@ZnO$  nanoparticles (0.5g) were dispersed in 100 ml water using mechanical stirring, then 0.2 ml of APTES was added to the mixture. During mechanical stirring, the reaction mixture was heated for two hours at  $70^{\circ}\text{C}$ . After cooling, it was extracted by magnetic filtration and washed three times with ethanol then dried at  $60^{\circ}\text{C}$  for 24 hours in an oven (Liu *et al.*, 2013).

#### Anticancer drug (DOX) loading

For drug loading, DOX was dissolved in PBS solution at a concentration of 0.0005 mg/L, then 60 mg of  $\text{Fe}_3\text{O}_4@ZnO$  nanoparticles were dispersed in 12 ml of this solution (0.01 mol). Using mechanical stirring, the mixture was stirred for 24 h under dark conditions and then collected by

centrifugation to obtain DOX-loaded Fe<sub>3</sub>O<sub>4</sub>@ZnO (Yu and Zhu, 2016).

$$\text{Drug Loading\%} = \frac{C_0 - C_s}{C_0} \times 100\%$$

Eq(1)

Where C<sub>0</sub> is the drug solution concentration before loading and C<sub>s</sub> is the concentration after loading.

### In vitro drug release

60 mg of drug-loaded zinc oxide and magnetite nanoparticles were dispersed in 10 ml buffer. Then, using mechanical stirring, the solution was agitated at 37°C, and the aliquots were centrifuged at specified intervals. The amount of drug released into the solution was estimated using the Shimadzu 2100S UV/Vis double beam recording spectrophotometer. The absorbance was measured at 490 nm every 60 min. The release percentage was calculated according to the following relation (2) (Ellis *et al.*, 2017; Unsoy *et al.*, 2014).

$$\text{Drug Release \%} = \frac{C_t}{C_0} \times 100\% \quad (2)$$

Where C<sub>t</sub> is the concentration at a specific time, C<sub>0</sub> is the initial concentration.

### Effect of ultrasonic on drug release

Fe<sub>3</sub>O<sub>4</sub>@ZnO loaded with DOX drug was allowed to release DOX under the effect of ultrasonic. 60 mg Fe<sub>3</sub>O<sub>4</sub>@ZnO loaded with DOX drug was dispersed in 10 ml buffer solution (pH = 7.4) and subjected to ultrasonication. The amount of drug released into the solution was estimated using UV-Vis spectrophotometry. The

absorbance was followed at 490 nm every 20 min (Cheung and Neyzari, 1984; Deng *et al.*, 2016; Jain *et al.*, 2018).

### In vitro drug release kinetics

Zero-order, First-order, Higuchi, Korsmeyer–Pappas, and Hixson–Crowell models kinetic equations were tested to assess the mechanism of drug in vitro release. Correlation coefficient R<sup>2</sup> was obtained from the drawing paragraph in pH 7.4 buffer (Mhlanga, *et al.*, 2015; Gouda, *et al.*, 2017; Fu and Kao, 2010).

## Results

### Analysis of the morphology and size of different synthesized drug delivery system (DDS) components

Scanning electron microscopy SEM images for magnetite formed by sonication method showed a uniform particle with a uniform average size of 25±5 nm as shown in Fig. 1 A. Fe<sub>3</sub>O<sub>4</sub>@ZnO SEM image is given in Fig. 1B. Obviously, the surface morphology shows the presence of the drug on its surface as a small white dots with no aggregation. The average size of Fe<sub>3</sub>O<sub>4</sub>@ZnO@DOX nanoparticles is about 120 ± 10 nm.

Low and high-resolution transmission electron microscopy (TEM) images for Fe<sub>3</sub>O<sub>4</sub>@ZnO nanoparticles loaded with DOX drug are shown in Fig. 2. The images demonstrate spherical shape of the core-shell system. The images also show a uniform size of the core-shell. The core magnetite size is 25±5 nm with the loaded drug appearing in a white color circumference.

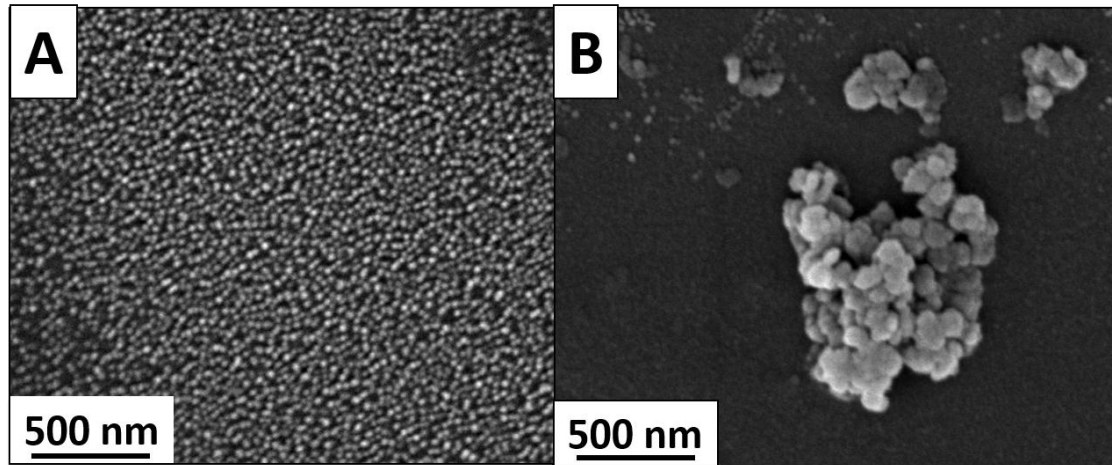


**Fig. 1:** SEM images for (A) magnetite (B) magnetite zinc oxide nanoparticles ( $\text{Fe}_3\text{O}_4@\text{ZnO}$ )

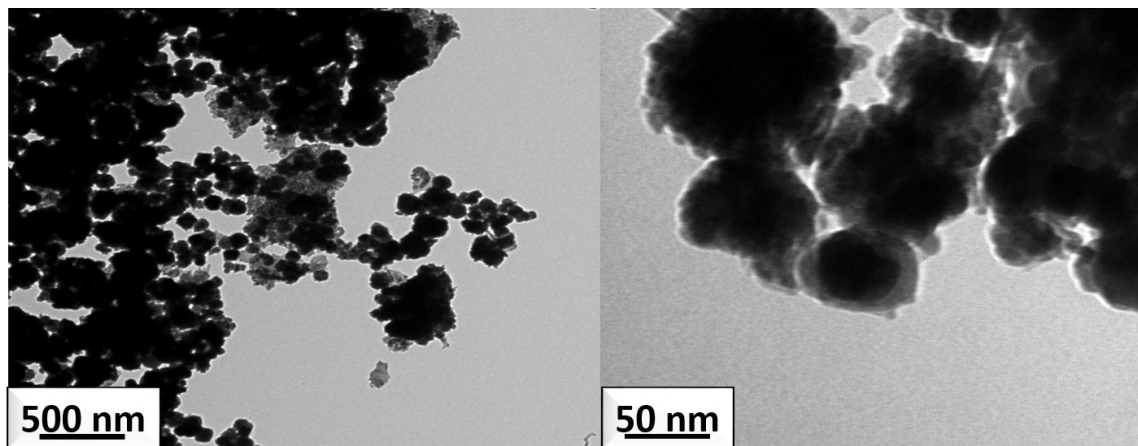


**Fig. 2:** Low and High-resolution TEM images for magnetite zinc oxide nanoparticles ( $\text{Fe}_3\text{O}_4@\text{ZnO}$ )

### ICP-OES and EDX analysis

ICP-OES was used to estimate the quantity of Zn loaded on the magnetite nanoparticles which was estimated by inductively coupled plasma (ICP) as  $163.8 \text{ mg g}^{-1}$ . Moreover, the presence of zinc was confirmed using energy dispersive X-ray (EDX) analysis. EDX measurements given in Fig. 3 indicate that iron and zinc are present in weight percentages of 37.59% and 1.26% respectively. The white dots on the SEM image are assigned to DOX drug that

is rich in carbon, oxygen, and nitrogen. The weight percentages of C, N, and O are 22.38%, 4.94%, and 33.84%, respectively. The high proportions of oxygen and carbon in comparison with Zn and Fe are due to the presence of both APTES and DOX drug.

### FTIR of the $\text{Fe}_3\text{O}_4@\text{ZnO}$ delivery system.

FTIR has been used to retrieve the different functional groups of the prepared nanomaterials. Fig. 5 illustrates the overlay FTIR spectral peaks of  $\text{Fe}_3\text{O}_4$  and

Fe<sub>3</sub>O<sub>4</sub>@ZnO nanoparticles found in the range between 450 and 4000 cm<sup>-1</sup>. The peaks that appeared at 438, 455 cm<sup>-1</sup> and 1025 cm<sup>-1</sup> correspond to metal-oxygen (Zn-O), metal-oxygen-metal (Fe-O-Zn) and (Zn-O-Zn) bonds respectively, and hence confirm the preparation of zinc oxide and magnetite (**Hassan et al., 2017; Bisht et al., 2016**). The absorptions at 1395.25 cm<sup>-1</sup> and 1591.29 cm<sup>-1</sup> are due to the COO-Fe bond of the acetate group. Appearance of a broad peak at 3300 cm<sup>-1</sup> is for O-H from absorbed water (**Hong et al., 2008**). In Fig. 6 Functionalization of magnetite@ zinc oxide nanoparticles with APTES leads to show amine (NH<sub>2</sub>) groups on its surface by chemical condensation between the ethoxy (found in APTES) and OH groups (found on the surface of zinc oxide). The bending vibrations of amino groups were detected at 1638 cm<sup>-1</sup>, meaning that amino groups have been loaded on the surface of magnetite@ zinc oxide nanoparticles. This mechanism can be confirmed by the presence of peak at 2925 cm<sup>-1</sup> that can be characteristic of C-H stretching vibrations confirming the presence of propyl group. The drug can bind to the surface of the Fe<sub>3</sub>O<sub>4</sub> core-shell functional nanoparticles with ketones on the DOX drug (Schiff base condensation). After drug loading, the FTIR spectra showed a peak at 1366 cm<sup>-1</sup> which can be characteristic to adsorption of C-N bonds caused by the interaction of the amino group of the functionalized nanoparticles with the carbonyl group of doxorubicin. (**Sun et al., 2015; Sadighian et al., 2014**).

### **XRD of Fe<sub>3</sub>O<sub>4</sub>@ZnO and the ZnO nanoparticles .**

Fe<sub>3</sub>O<sub>4</sub>@ZnO nanoparticles were analyzed by XRD. Fig. 4 illustrates the XRD graphs of ZnO, magnetite (Fe<sub>3</sub>O<sub>4</sub>), and Fe<sub>3</sub>O<sub>4</sub>@ZnO nanoparticles. ZnO pattern has nine peaks indexed to the (100), (002), (101), (102), (110), (103), (200), (112), and (201) Miller indices, respectively (**Beltran-Huarac et al., 2010**). Sharp peaks in Fig. 4 suggest that ZnO NPs have been prepared with high crystallinity. In the case of Fe<sub>3</sub>O<sub>4</sub>, the (Fe<sub>3</sub>O<sub>4</sub>) pattern has six characteristic Miller indices peaks (110), (311), (400), (422), (511), and (440), respectively (**Beltran-Huarac et al., 2010**). All of the observed peaks in the sample have high crystallinity as revealed by strong sharp peaks. Similarly, the presence of ZnO nanoparticles on the surface of magnetite nanoparticles is confirmed by the XRD spectrum of magnetite coated with ZnO nanoparticles, where the peaks assigned to ZnO (101) and Fe<sub>3</sub>O<sub>4</sub> (311) nanoparticles were found (**Arvand and Daneshvar, 2019; Heuser et al., 2007**). This is consistent with the composition of the core/shell Fe<sub>3</sub>O<sub>4</sub>@ZnO. The average crystallite size of the core/shell was estimated by using the Scherrer equation, using the diffraction of the most intense peak (101) for ZnO which is about 24.6 nm (**Singh et al., 2020; Elshypany et al., 2021; Huarac et al., 2010**).

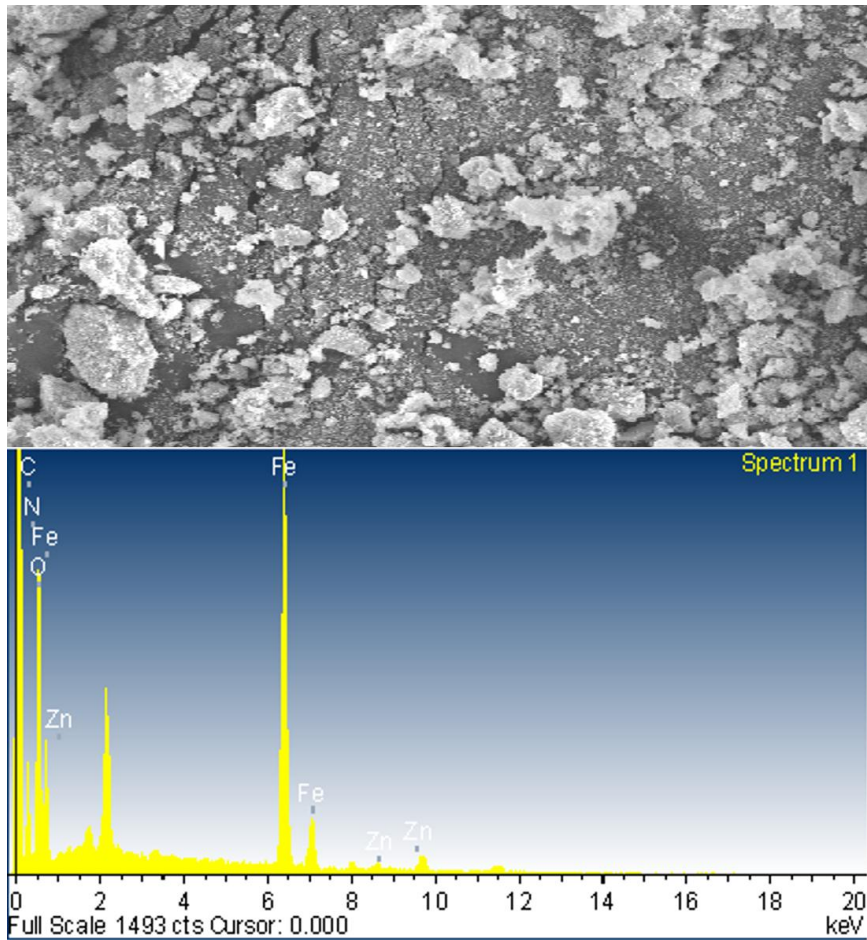


**Fig. 3:** EDX results of magnetite zinc oxide nanoparticles after loading with drug

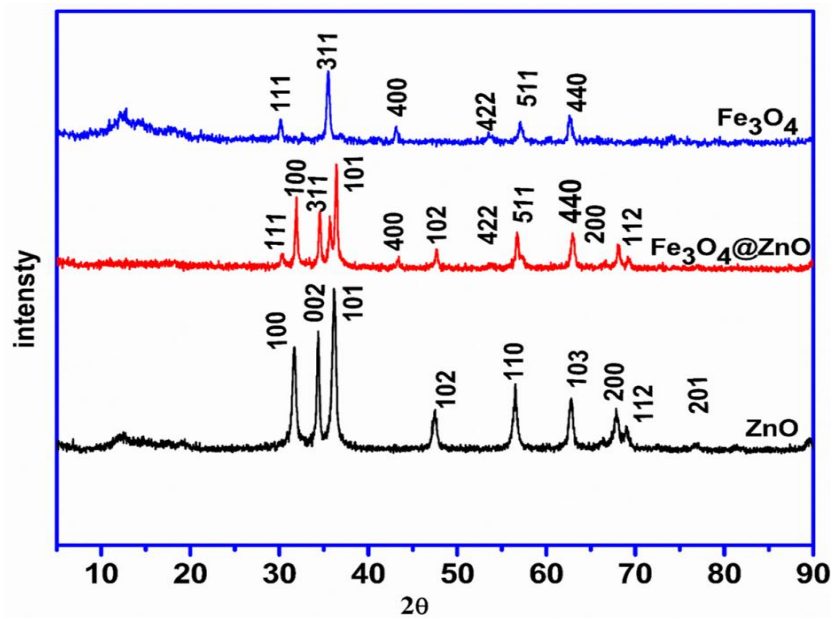


**Fig. 4:** XRD pattern of zinc oxide, magnetite zinc oxide and magnetite nanoparticles.

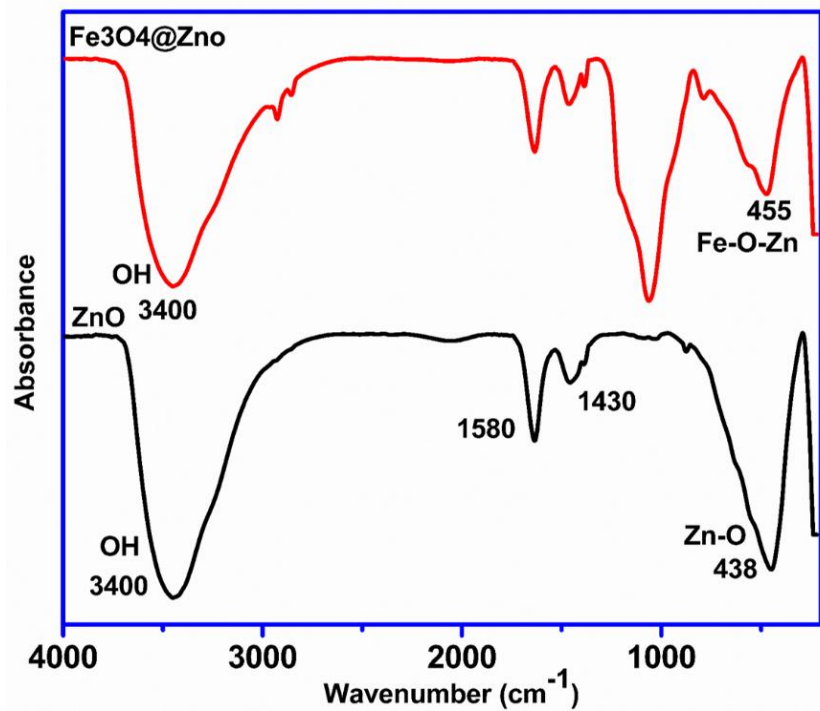


**Fig. 5:** FTIR pattern for zinc oxide and magnetite zinc oxide nanoparticles.

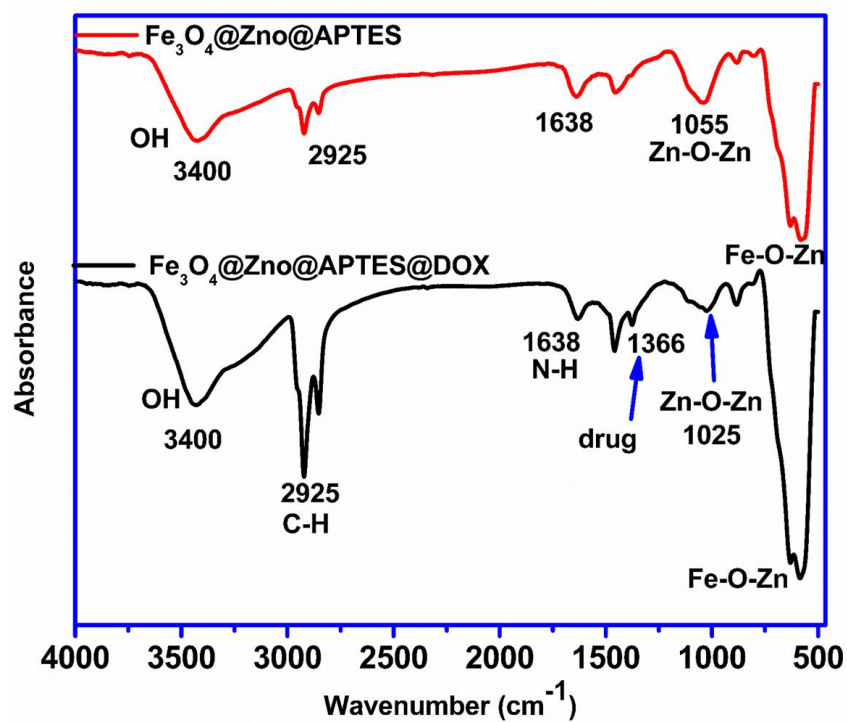


**Fig. 6:** FTIR pattern for magnetite@ zinc oxide @APTES and magnetite@ zinc oxide @APTES@DOX nanoparticles.

### Magnetization measurements

Vibrating sample magnetometry (VSM) ranging from  $-10$  kOe to  $+10$  kOe for the synthesized  $\text{Fe}_3\text{O}_4@ZnO$  nanoparticles was performed. Fig. 7 shows the saturation magnetization values, deduced from the hysteresis loop for uncoated  $\text{Fe}_3\text{O}_4@ZnO$  sample as  $5.9$  emu/g. The saturation magnetization value decreased after coating  $\text{Fe}_3\text{O}_4@ZnO$  with APTES reaching  $5.3$ . The value decreased further to  $1.6$  emu/g upon DOX drug loading. The decrement in value of magnetization after

casing with zinc oxide in all the patterns is normal due to the formation of three layers of zinc oxide, APTES, and DOX drug around the magnetite core. Another possible reason for this deviation could be because of the formation of chemical chains like (Fe-O-Zn) during functionalization with ZnO. As a result, a decrease and perhaps even disappearance of the magnetic moment of magnetite may occur (Abbas *et al.*, 2014).

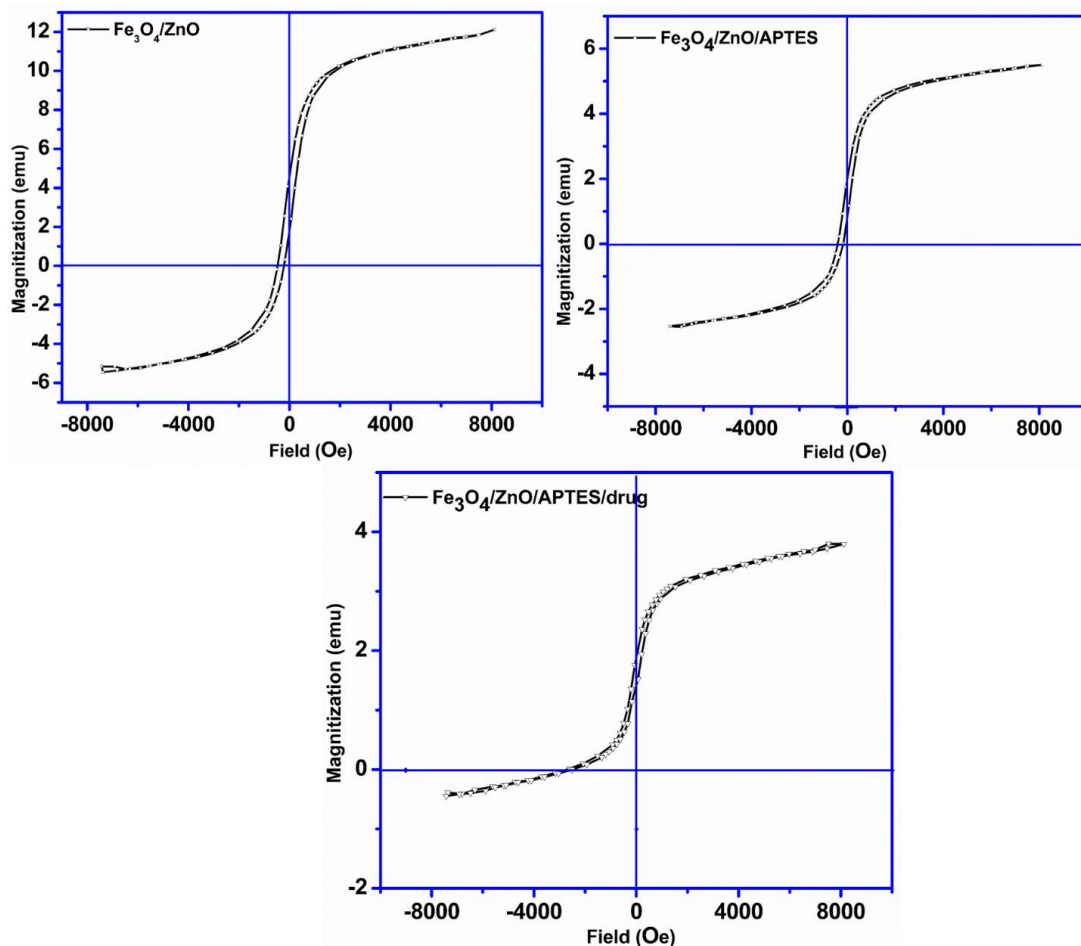


**Fig.7:** The magnetization curves for  $\text{Fe}_3\text{O}_4@ZnO$  nanoparticles,  $\text{Fe}_3\text{O}_4@ZnO@APTES$ , and  $\text{Fe}_3\text{O}_4@ZnO@APTES@drug$  after loading with drug measured by VSM

## Thermogravimetric analysis (TGA) and loading efficiency

Thermogravimetric analysis is usually performed to evaluate the thermal behavior and thermal stability of nanoparticles during the heating process to confirm the coating formation and to estimate the binding of the drug on the surface of the magnetite zinc oxide nanoparticles. Fig. 8 shows the TGA and DTGA thermograms of parent  $\text{Fe}_3\text{O}_4@ZnO$ ,  $\text{Fe}_3\text{O}_4@ZnO$  functionalized with APTES and finally  $\text{Fe}_3\text{O}_4@ZnO@APTES$  loaded with DOX drug in the temperature range of 30–700°C. The weight loss occurred in three stages. Stage one below 200°C corresponding loss of moisture and ethanol solvent (Qiao *et al.*, 2015). Stage two from 200–400°C indicates the decomposition of the amino groups

coming from APTES. Stage three in the range 400–800°C indicating the decomposition of organic matter coming from loaded drug (Abbas *et al.*, 2014). The percentage of the drug (DOX) could be calculated by comparing the weight loss from 300°C to 700°C in both ( $\text{Fe}_3\text{O}_4@ZnO@APTES$ ) and ( $\text{Fe}_3\text{O}_4@ZnO@APTES@DOX$ ) samples. According to Fig. 8, the weight loss from 300 to 700°C in the DOX loaded particles was about 18.07% and that for the unloaded particles was about 12.5%. Therefore, it was found that 5.57 µg DOX are loaded per mg of  $\text{Fe}_3\text{O}_4@ZnO$  functionalized nanoparticles (Gemeay *et al.*, 2017).

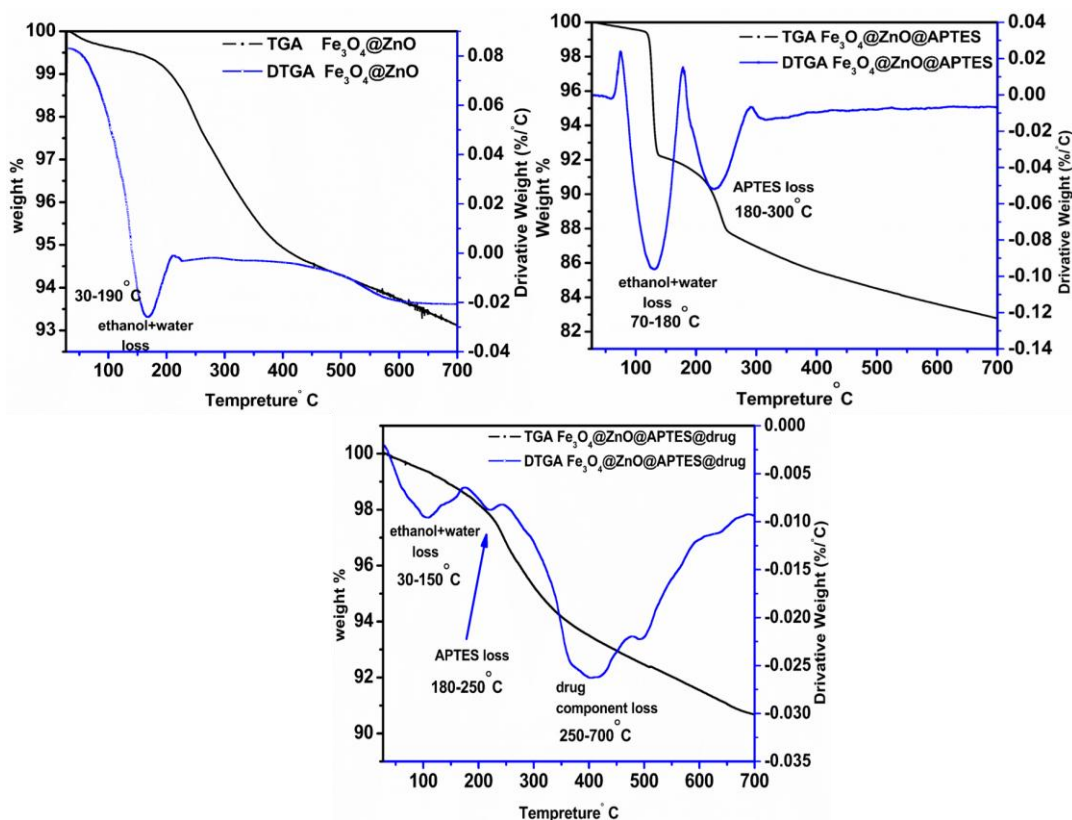


**Fig. 8:** TGA curves for magnetite zinc oxide nanoparticles after functionalization and loading DOX

## Evaluation of the in vitro drug release patterns

Control releasing of DOX drug loaded on the surface of Fe<sub>3</sub>O<sub>4</sub>@ZnO nanoparticles was studied in vitro in phosphate buffer solution at pH 7.4. The kinetics of drug release was studied by applying first-order, zero-order, Hixson-Crowell, Higuchi, and Korsmeyer-Peppas models using Fe<sub>3</sub>O<sub>4</sub>@ZnO@APTES loaded with 500 ppm DOX drug.

A Zero-order model (Eq.S1) is a model used to describe the drug-releasing from pharmaceutical dosage systems having a cohesive nature and the drug releases slowly from the system with no disaggregation (Mhlanga and Ray, 2015).

The first-order model (Eq. S2) describes the elimination of certain drugs from the system. In First order model, releasing is dependent on the concentration of drug meaning that the greater the concentration, the faster drug releases.

The Higuchi equation (Eq. S3) is an important kinetic equation that studies drug diffusion mechanisms from drug delivery development systems. The obtained data were plotted as a graph of % of drug release on the x-axis versus  $t^{1/2}$  on the y-axis and when a straight line is obtained, its slope will be equal to the Higuchi dissolution constant ( $k_H$ ) and it can be said that the system follows the kinetics of  $t^{1/2}$  model.

The Hixson-Crowell model (Eq. S4) characterizes drug liberation from systems in which drug-carrying particle size changes. Therefore, the size of these particles is directly proportional to the cube root of drug

release by decomposition, not by diffusion. So Hixson-Crowell found a relevance between time and the release of medicine from the concept above. A graph (the cube root of drug remaining) is plotted on the y-axis versus time on the x-axis to study release kinetics (Mhlanga and Ray, 2015; Gouda *et al.*, 2017).

Korsmeyer-Peppas model (Eq. S5) is one of the most important relationships describing drug release from a polymeric system. Hence, the value of (n) in this relationship can be used to characterize the different mechanisms of drug release for spherical systems (Table 1, S5). To discuss the kinetics of release, a diagram is drawn between the cumulative percent logarithms of drug releases ( $\log (M_t / M_\infty)$ ) versus log time ( $\log t$ ). The value of n can be extracted from the graph by which different editing mechanisms can be distinguished as given in the tabular form (Table 1, S5). Table 1 shows that n is less than 0.43, which is evidence that the developed system follows the dissolution, not the diffusion mechanism.

Finally, the calculations indicated that DOX drug release from Fe<sub>3</sub>O<sub>4</sub>@ZnO nanoparticles follows zero-order with a higher correlation coefficient  $R^2 = 0.98$  that is higher than  $R^2$  for other models. This means that drug release from the Fe<sub>3</sub>O<sub>4</sub>@ZnO@APTES@DOX system follows zero-order kinetics whereby drug release rate is independent of concentration, and the dissolution mechanism is dominant mechanism. (Table 1 and Figs. 9, 10) (Gouda, *et al.*, 2017).

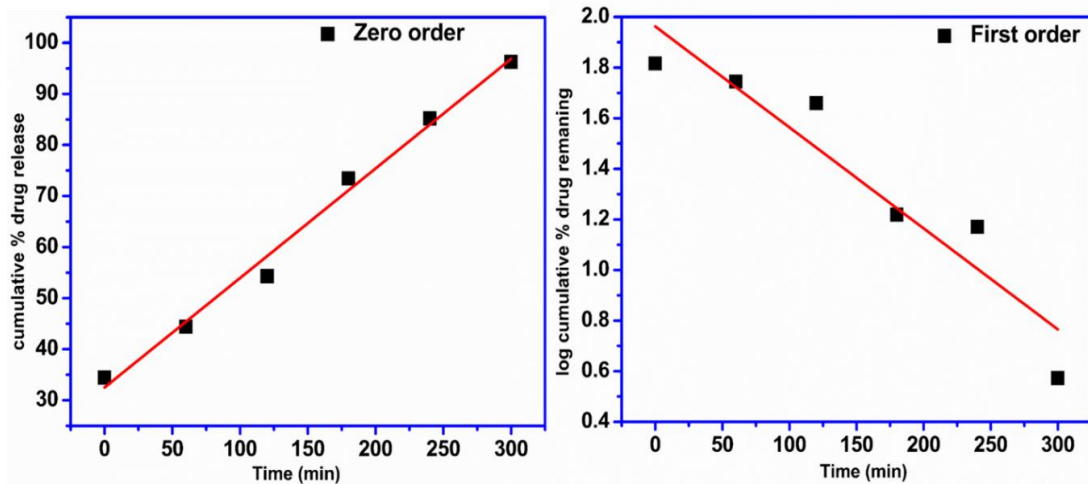


**Fig. 9:** First-order, Zero-order model for magnetite zinc oxide nanoparticles at pH=7.4 using mechanical stirring.

**Table 1:** Release kinetics control of DOX loaded Fe<sub>3</sub>O<sub>4</sub>@ZnO at pH=7.4 using mechanical stirring

Fe <sub>3</sub> O <sub>4</sub> /ZnO	Zero Order		First Order		Higuchi Model		Korsmyer-Peppas Model			Hixson -Crowel Model	
	R <sup>2</sup>	K <sub>1</sub>	R <sup>2</sup>	K <sub>2</sub>	R <sup>2</sup>	K <sub>3</sub>	R <sup>2</sup>	K <sub>4</sub>	N	R <sup>2</sup>	K <sub>5</sub>
pH=7.4	0.98	0.21	0.86	-0.006	0.85	2.8	0.85	1	0.36	0.92	1.08

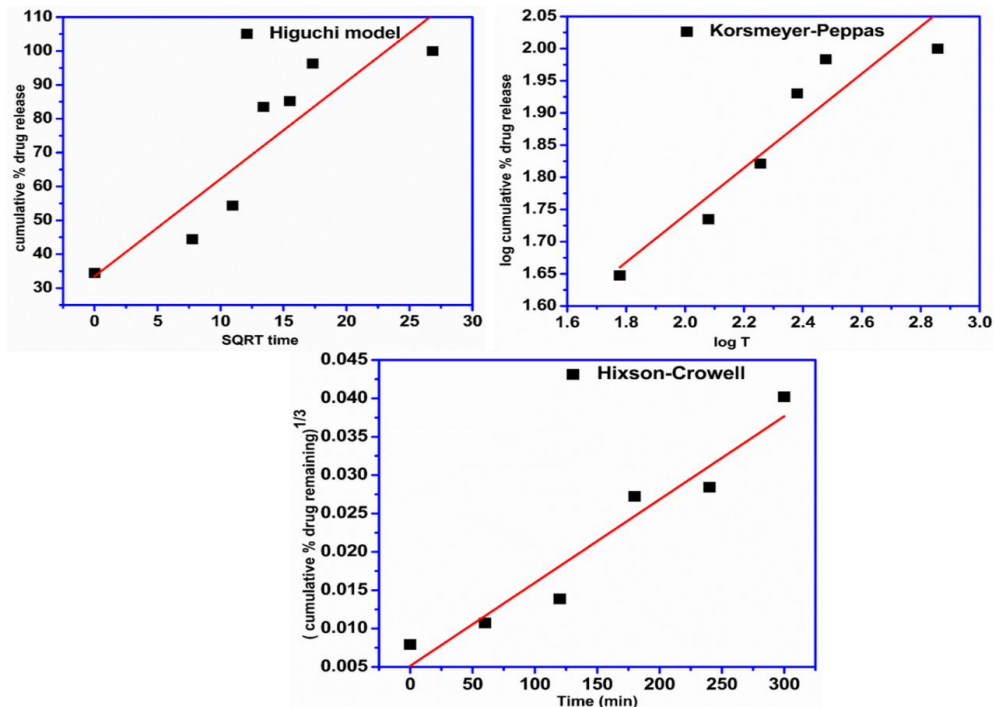


**Fig. 10:** Korsmeyer-Peppas, Higuchi model and Hixson-Crowell model for magnetite zinc oxide nanoparticles at pH=7.4 using mechanical stirring.

### **Kinetics of drug release using ultrasonication**

Ultrasonication was applied as a stimulus for DOX drug release from  $\text{Fe}_3\text{O}_4@\text{ZnO}@\text{APTES}@\text{DOX}$  core-shell system at  $37^\circ\text{C}$  (Qiao *et al.*, 2015; Gemeay *et al.*, 2017). The kinetics of DOX drug release have been studied applying zero-order, first-order, Higuchi, Hixson-Crowell, and Korsmeyer-Pappas models. For each model, ( $R^2$ ), ( $n$ ), and ( $k$ ) were evaluated to assess the kinetic release mechanisms of the drug. Plots are shown in Figs.11, 12 and values are given in Table 2. DOX drug release from  $\text{Fe}_3\text{O}_4@\text{ZnO}-\text{APTES} / \text{DOX}$  core-shell was found to follow Zero-order kinetics ( $R^2 = 0.97$ ) with a dominating dissolution mechanism. Another important result is that the time of drug-release upon using ultrasonication is five times faster than that caused by mechanical stirring under the same experimental conditions.

### **Conclusion**

The system in this study has been developed by using the ultra-sonication preparation method. It is composed of magnetite ( $\text{Fe}_3\text{O}_4$ ) as a core and zinc oxide as a shell, then decorating this system with aminopropyl tetraethyl orthosilicate (APTES) and loading with doxorubicin

anticancer drug (DOX). Doxorubicin is an anticancer used for treating breast cancer. The mean particle size of this system was determined using scanning electron microscopy as about  $120\pm 10$  nm. Transmission electron microscopy showed the formation of core magnetite and shell zinc oxide with loaded DOX drug as small dots on the system's surface. The magnetization value for magnetite / zinc oxide nanoparticles is about 5.3 emu/g that decreases after functionalization with APTES and decreases further upon loading with DOX down to 1.6 emu/g. The loaded amount of the drug is 0.093  $\mu\text{mol}$  which is considered suitable for biological applications, as it can be viewed as an appropriate amount that does not cause cytotoxicity and at the same time treats the affected area. The releasing of drug was found to follow zero-order kinetics at  $\text{pH} = 7.4$  in both mechanical and ultrasonic releasing methods. In vitro kinetic release showed an excellent enhanced release under exposure to ultrasonic. The time of drug-release upon using ultrasonic is five times faster than that caused by mechanical stirring under the same experimental conditions.

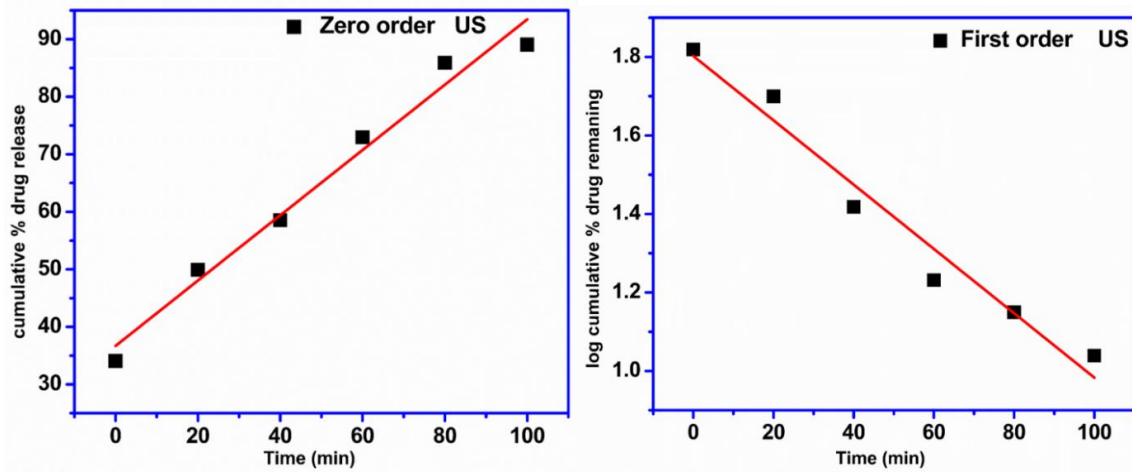


Fig. 11: Zero-order model and first-order model for magnetite zinc oxide nanoparticles at pH=7.4 by using ultrasonic

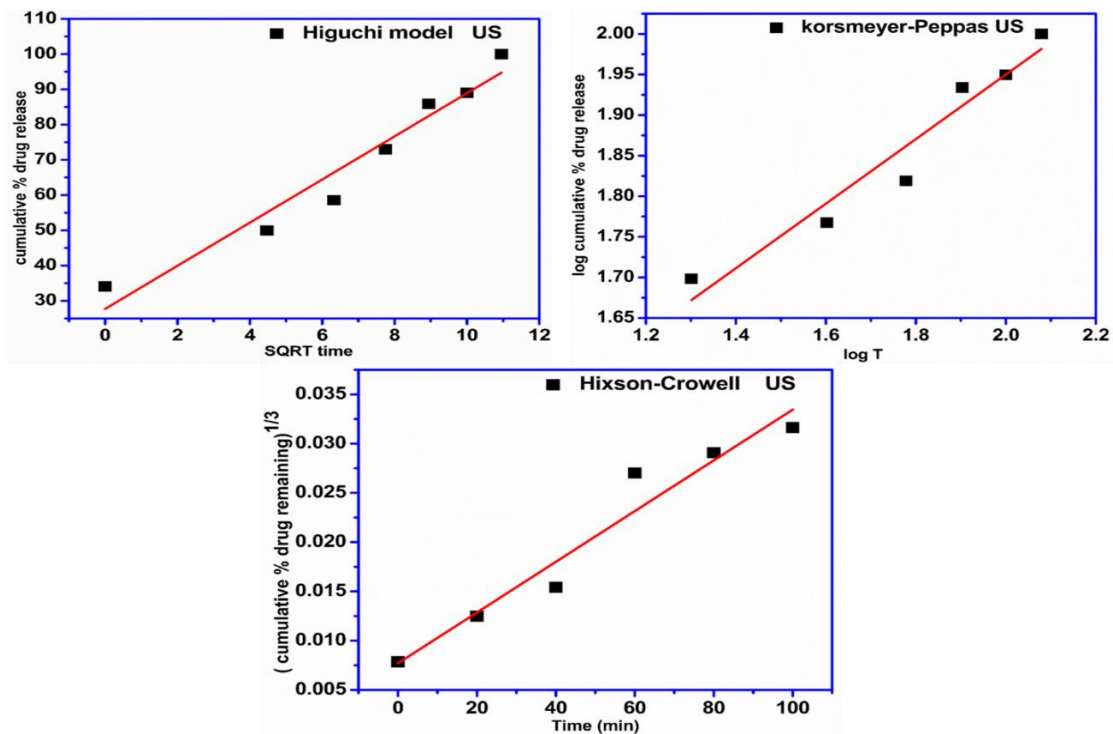


Fig. 12: Higuchi model, Korsmeyer-Peppas and Hixson-Crowell model at pH=7.4 using ultrasonic.

Table 2: Controlled kinetic drug release for Fe<sub>3</sub>O<sub>4</sub>/ZnO using ultrasonic

.Ultrasonic	Zero order		First order		Higuchi Model		Krosmyer-Peppas Model			Hixson-Crowell Model	
	R <sup>2</sup>	K <sub>1</sub>	R <sup>2</sup>	K <sub>2</sub>	R <sup>2</sup>	K <sub>3</sub>	R <sup>2</sup>	K <sub>4</sub>	N	R <sup>2</sup>	K <sub>5</sub>
Fe <sub>3</sub> O <sub>4</sub> /ZnO	0.97	0.56	0.95	-.04	0.93	6.12	0.92	1.15	0.39	0.93	2.57

## Reference

- Abbas, M.; Takahashi, M. and Kim, C., (2013).** Facile sonochemical synthesis of high-moment magnetite ( $\text{Fe}_3\text{O}_4$ ) nanocube. *J. Nanoparticle Res.*, 15(1): 1-12.
- Abbas, M.; Torati, S.R.; Soo, L.C.; Rinaldi, C. and Kim, C., (2014).**  $\text{Fe}_3\text{O}_4/\text{SiO}_2$  core/shell nanocubes: novel coating approach with tunable silica thickness and enhancement in stability and biocompatibility. *J. Nanomed Nanotech.*, 5(6): 1-8.
- Arvand, M. and Daneshvar, S., (2019).** Facile Strategy for Preparation of Core/Shell-structured Zinc Oxide-magnetite Hybrids for Quantification of Quercetin and Rutin in Pharmaceutical Herbs. *J. Anal. Chem.*, 74(9): 920-932.
- Beltran-Huarac, J.C.; Singh, S.P.; Tomar1, M.S.; Peña, S. and Rivera, S., (2010).** Synthesis of  $\text{Fe}_3\text{O}_4/\text{ZnO}$  core-shell nanoparticles for photodynamic therapy applications. *MRS Online Proc. Libr. Arch.*, 1257: 4-6.
- Bisht, G.; Rayamajhi, S.; Biplab K.c.; Nath, P.S.; Karna, K.; Shrestha, B.G., (2016).** Synthesis, Characterization, and Study of In Vitro Cytotoxicity of  $\text{ZnO-Fe}_3\text{O}_4$  Magnetic Composite Nanoparticles in Human Breast Cancer Cell Line (MDA-MB-231) and Mouse Fibroblast (NIH 3T3). *J. Nanoscale Res. Lett.*, 11.
- Cheung, A.Y. and Neyzari, A., (1984).** Deep local hyperthermia for cancer therapy: external electromagnetic and ultrasound techniques. *J. Cancer Res.*, 44(10 Supplement): 4736s-4744s.
- Deng, Z.; Xiao, Y.; Pan, M.; Li, F.; Duan, W.; Meng, L.; Liu, L.; Yan, F.; Zheng, H., (2016).** Hyperthermia-triggered drug delivery from iRGD-modified temperature-sensitive liposomes enhances the anti-tumor efficacy using high intensity focused ultrasound. *JCR*, 243: 333-341.
- Ellis, E.; Zhang, K.; Lin, Q.; Enyi Ye; Poma, A.; Battaglia, G.; Loh, X.J. and Lee, T., (2017).** Biocompatible pH-responsive nanoparticles with a core-anchored multilayer shell of triblock copolymers for enhanced cancer therapy. *JMCBDV*, 5(23): 4421-4425.
- Elshypany, R.; Selim, H.; Zakaria, K.; Moustafa, A.H.; Sadeek, S.A.; Sharaa, S.; Raynaud, P.; Nada, A.A., (2021).** Magnetic ZnO Crystal Nanoparticle Growth on Reduced Graphene Oxide for Enhanced Photocatalytic Performance under Visible Light Irradiation. *J. MOLE*, 26(8): 2269.
- Fu, Y. and W.J. Kao, (2010).** Drug release kinetics and transport mechanisms of non-degradable and degradable polymeric delivery systems. *Expert opinion on drug delivery*, 7(4): 429-444.
- Gemeay, A.H.; El-Halwagy, M.E.; El-Sharkawy, R.G.; Zaki, A.B., (2017).** Chelation mode impact of copper (II)-aminosilane complexes immobilized onto graphene oxide as an oxidative catalyst. *J. Environ. Chem. Eng.* 5(3): 2761-2772.
- Gouda, R.; Baishya, H. and Qing, Z. (2017).** Application of mathematical models in drug release kinetics of carbidopa and levodopa ER tablets. *J. Dev. Drugs*, 6(02): 1-8.

- Hassan, H.S.; Elkady, M.F.; Amer, W.A.; Salama, E.; Algarni, H. and Shaaban, E.R., (2017).** Fabrication of novel magnetic zinc oxide cellulose acetate hybrid nano-fiber to be utilized for phenol decontamination. *J. Taiwan Inst. Chem. Eng.*, 78: 307-316.
- Heuser, J.; Spindel, W. U.; Pisarenko, A. N.; Yu, C.; Pechan, M. J.; Pacey, G. E., (2007).** Formation of surface magnetite nanoparticles from iron-exchanged zeolite using microwave radiation. *J. Mater. Sci.*, 42(21): 9057-9062.
- Hong, R.Y., Zhanga, S.Z., Dic, G.Q., Lib, H.Z., Zhengd, Y., Dinge, J., Wei, D.G. (2008).** Preparation, characterization and application of Fe<sub>3</sub>O<sub>4</sub>/ZnO core/shell magnetic nanoparticles. *J. Mater. Res. Bull.* 43(8-9): 2457-2468.
- Huarac, J.C.B., Tomar, M .S. Singh, S.P., Oscar Perales-Perez, Rivera, L., and Peña, S., (2010).** Multifunctional Fe<sub>3</sub>O<sub>4</sub>/ZnO core-shell nanoparticles for photodynamic therapy. In NSTI-Nanotech.
- Jain, A., Tiwari, A., Verma, A., Jain, S.K., (2018).** Ultrasound-based triggered drug delivery to tumors. *Drug Deliv. Transl. Res.*, 8(1): 150-164.
- Keshavarz, H., Khavandi, A., Alamolhoda, S., and Naimi-Jamal, M.R., (2020).** Ph-Sensitive magnetite mesoporous silica nanocomposites for controlled drug delivery and hyperthermia. *RSC Advances*, 10(64): 39008-39016.
- Liu, Y., Li, Y., Li, X., He, T., (2013).** Kinetics of (3-aminopropyl) triethoxysilane (APTES) silanization of superparamagnetic iron oxide nanoparticles. *Langmuir*, 29(49): 15275-15282.
- Mhlanga, N. and S.S. Ray, (2015).** Kinetic models for the release of the anticancer drug doxorubicin from biodegradable polylactide/metal oxide-based hybrids. *Int. J. Bio. Macromol.*, 72: 1301-1307.
- Moorthy, M.S., Subramanian, P., Panchanathan, M., Mondal, S., Kim, H., Lee, K.D., and Junghwan, (2017).** Fucoidan-coated core-shell magnetic mesoporous silica nanoparticles for chemotherapy and magnetic hyperthermia-based thermal therapy applications. *NJC*, 41(24): 15334-15346.
- Qiao, B., Wang, T., Gao, H., Jin, Y., (2015).** High density silanization of nano-silica particles using  $\gamma$ -aminopropyltriethoxysilane (APTES). *J. Appl. Surf. Sci.*, 351: 646-654.
- Sadighian, S., Rostamizadeh, K., Hosseini-Monfared, H., Hamidi, M., (2014).** Doxorubicin-conjugated core-shell magnetite nanoparticles as dual-targeting carriers for anticancer drug delivery. *J. Colloids Surf. B*117: 406-413.
- Shen, M., Cai, H., Wang, X., Cao, X., Li, K., Wang, S.H., Guo, R., Zheng, L., Zhang, G., Shi, X., (2012).** Facile one-pot preparation, surface functionalization, and toxicity assay of APTES-coated iron oxide nanoparticles. *Nanotechnology*, 23(10): 105601.
- Singh, H., Kuma, A., Thakur, A., Kumar, P., Nguyen, V., Dai-Vie, N., VO, Sharma, A., Kumar, D., (2020).** One-pot synthesis of magnetite-ZnO nanocomposite and its photocatalytic activity. *J. Top Catal.*, 63(11): 1097-1108.
- Sun, L., Hu, S., Sun, H., Guo, H., Zhu, H. Liu, M., Sun, H., (2015).** Malachite

- green adsorption onto  $\text{Fe}_3\text{O}_4@ \text{SiO}_2\text{-NH}_2$ : isotherms, kinetic and process optimization. *RSC Advances*, 5(16): 11837-11844.
- El-Alaily, T.M.; El-Nimr, M.K.; Kamel, M.M.; Meaz, T.M.; Asser, S.T., (2015).** Construction and celebration of low cost and fully automated vibrating sample magnetometer. *J. Mag. and Mag.Matererials*, 386:25-30.
- Unsoy, G.; Khodadust, R.; Yalcin, S.; Mutlu, P.; Gunduz, U., (2014).** Synthesis of Doxorubicin loaded magnetic chitosan nanoparticles for pH responsive targeted drug delivery. *European J. Pharm. Sci.*, 62: 243-250.
- Watermann, A. and J. Brieger, (2017).** Mesoporous silica nanoparticles as drug delivery vehicles in cancer. *Nanomaterials*, 7(7): 189.
- Xiao, Q. and C. Xiao, (2009).** Preparation and characterization of silica-coated magnetic-fluorescent bifunctional microspheres. *N.R. Let.*, 4(9): p. 1078-1084.
- Yi, G.C.; Wang, C. and Park, W.I. (2005).** ZnO nanorods: synthesis, characterization and applications. *Semiconductor. J. Sci. Technol.* 20(4): S22.
- Yu, X. and Y. Zhu, (2016).** Preparation of magnetic mesoporous silica nanoparticles as a multifunctional platform for potential drug delivery and hyperthermia. *J. Sci. Technol. Adv. Mater.*, 17(1): 229-238.
- Zada, A.; Ahmed, M.; Anninga, B.; Baker, R.; Kusakabe, M.; Sekino, M.; Klaase, J. M.; Haken, B.T.; Douek, M., (2016).** Meta-analysis of sentinel lymph node biopsy in breast cancer using the magnetic technique. *BJS*, 103(11): 1409-1419.

## تطوير أكسيد الزنك المغناطيسي لتطبيقه في مجال توصيل الدواء

أ.د/الزيني موسى عبيد- أ.د/ محمد يسري الشيخ -د/ عبد الحميد محمد الصاوي، حورعزب

قسم الكيمياء- كلية العلوم- جامعة طنطا

اجتذب تطوير نظام توصيل الأدوية لاستهداف المناطق المريضة اهتماماً كبيراً. حيث من المفترض أن يحقق النظام تأثيره العلاجي المرغوب دون آثار جانبية. تُظهر الجسيمات النانوية  $\text{ZnO}$  جهوداً كبيرة في العلاج الضوئي (PDT)، نظراً لقدرتها على توليد أنواع الأكسجين التفاعلية (ROS)، من المتوقع أن تموت الخلايا السرطانية دون الإضرار بالخلايا الصحية.

يضم هذا البحث نظاماً مطوراً لإيصال الدواء هو نظام الجسيمات النانوية لأكسيد الزنك المغنتيت ( $\text{Fe}_3\text{O}_4@ \text{ZnO}$ ). أظهر الفحص المجهر الإلكتروني (SEM) تكوين المغنتيت بجسيم نانوي كروي موحد بحجم قلب يساوي  $25 \pm 5$  نانومتر. يبلغ متوسط حجم الجسيمات النانوية لأكسيد الزنك المغنتيت ( $\text{Fe}_3\text{O}_4@ \text{ZnO}$ ) بعد التنفيع باستخدام (3-أمينوبروبيل) ثلاثي إيثوكسيل سيلان (APTES) وتحميل الدواء حوالي  $120 \pm 10$  نانومتر. تُظهر صورة المجهر الإلكتروني للإرسال (TEM) الحجم الموحد للقشرة الأساسية. الحجم الأساسي للمغنتيت يساوي  $25 \pm 5$  نانومتر، ولغلاف أكسيد الزنك يساوي  $95$

± ١٥ نانومتر. لتقليد درجة الحموضة في الدم ، تمت دراسة إطلاق الدواء في محلول عازل الفوسفات (PBS) عند درجة الحموضة ٧.٤.

إلى لى جانب طريقة التحريك الميكانيكي ، تم استخدام الموجات فوق الصوتية كمحفزات خارجية لإطلاق الدواء. تم وضع وزن ثابت من Fe<sub>3</sub>O<sub>4</sub>@ZnO المحمل بالدواء في محلول (الرقم الهيدروجيني = ٧.٤). بعد ذلك ، تم تحريكه باستخدام الموجات فوق الصوتية. ودراسه حركيه هذا النظام وجدنا انه يتبع الحركية الصفيرية في كل من المحفزات الخارجية.

في الختام ، تم تصنيع النظام المطور كنظام توصيل الدواء علي شكل قلب / صدفة باستخدام طريقة الموجات فوق الصوتية. وقد وجد انه وقت إطلاق الدواء عند استخدام ultrasonicaion أسرع بخمس مرات من الوقت الناتج عن التحريك الميكانيكي في نفس الظروف التجريبية.